Research Square

Preprints are preliminary reports that have not undergone peer review.
They should not be considered conclusive, used to inform clinical practice,
or referenced by the media as validated information.

Germinal Centers Function as Macromolecular Sanctuaries that Protect Follicular T Cells from Immunotoxin-Mediated Depletion

Shihyoung Kim
The Ohio State University https://orcid.org/0000-0002-8846-2853
Rajni Kant Shukla
The Ohio State University
Sarah Golconda
The Ohio State University
Hannah Yu
The Ohio State University
John C. Reneau
The Ohio State University
Namal P. M. Liyanage
The Ohio State University
Walter Hanel
The Ohio State University
Sanggu Kim
kim.6477@osu.edu
The Ohio State University https://orcid.org/0000-0003-1228-6168

Research Article

Keywords: Immunotherapy, CD3 immunotoxin, T-cell depletion, germinal center, follicular T helper cells, tissue barrier

Posted Date: November 6th, 2026

DOI: https://doi.org/10.21203/rs.3.rs-11628345/v1

License: This work is licensed under a Creative Commons Attribution 4.0 International License.
Read Full License

Additional Declarations: The authors declare potential competing interests as follows: SK (Shihyoung), SK (Sanggu) and JCR have submitted an invention disclosure to The Ohio State University related to immunotoxin technology described in this manuscript. No patent application, licensing agreement, royalty arrangement, or other financial interest has resulted from this disclosure as of the date of submission. The remaining authors declare no competing interests.

Abstract

Targeted lymphodepletion with CD3 immunotoxins (CD3-ITs) is promising for transplantation and T-cell malignancies, but incomplete tissue depletion limits efficacy. We used a murine anti-CD3 immunotoxin model, intravascular staining, histology, and CD4-iDTR mice to define factors associated with survival of follicular T cells. CD3-IT caused profound systemic T-cell depletion and enrichment of follicular helper (T_{FH}) and follicular regulatory (T_{FR}) T cells among surviving $CD4^+$ cells in spleen, Peyer's patches, and lymph nodes. Ex vivo, $CXCR5^+$ T cells bound CD3-IT comparably to $CXCR5^-$ cells and showed similar susceptibility to CD3-IT-mediated cytotoxicity (IC_{50}, 0.471–0.569 nM). In contrast, within the splenic parenchyma, $CXCR5^+$ T cells bound CD3-IT at approximately half the level of $CXCR5^-$ counterparts ($p < 0.05$). Histologically, CD3-IT depleted 83% of T cells in splenic T-cell zones, whereas GC T cells were relatively spared. Fc-silent anti-CD40L pretreatment disrupted GC architecture and was associated with a marked reduction in the phenotypic T_{FH} compartment after CD3-IT treatment. In CD4-iDTR mice, free diphtheria toxin (DT) and CD3-IT produced substantially less depletion of GC than T-cell-zone T cells, whereas Fc-silent anti-CD3 mAb down-modulated CD3 on GC-T_{FH} cells. BrdU incorporation did not indicate disproportionate GC-T_{FH} proliferation, and relative sparing with both a 58-kDa free DT and a 278-kDa CD3-IT indicates that size alone is insufficient to explain the effect in intact germinal centers *in vivo*. Together, these data show that intact GC architecture creates a functional barrier to toxin-mediated depletion of resident follicular T cells.

Introduction

To date, there is no curative therapy for most T-cell lymphomas. T-cell-targeting immunotoxins represent promising precision therapeutics for both cutaneous and peripheral T-cell lymphomas.[1, 2] Immunotoxin-mediated T-cell depletion has also shown preclinical efficacy in preventing allograft rejection [3–5] and treating autoimmune diseases.[6] While conventional monoclonal antibody (mAb)-mediated T-cell depletion is often inefficient for tissue-resident T cells—effector macrophages and granulocytes, essential for host Fc-receptor effector mechanisms, are often scarce within extravascular tissue parenchyma,—immunotoxins enable profound depletion of both circulating and tissue-resident T cells by delivering ribosomal-inactivating protein payloads directly into target cells, triggering cell-autonomous death.[7–9]

Recent immunotoxin regimens, including *Resimmune* (CD3-directed immunotoxins) and *denileukin diftitox* (IL-2R–targeted diphtheria-toxin fusions), have yielded notable clinical response rates in cutaneous T-cell lymphoma (CTCL); however, single-agent efficacy remains inconsistent and limited in peripheral T cell lymphomas (PTCLs) and advanced CTCLs due partially to variable target expression and suboptimal endocytic internalization.[1, 2] Furthermore, previous studies demonstrated that while $CD3^{dim}$ regulatory T cells (Tregs) are relatively spared after CD3-directed immunotoxin (CD3-IT) treatment, whereas tolerance-inducing $CD3^{hi}$ Tregs ($CD62L^{hi}$ naïve/quiescent Tregs)[10, 11] are profoundly

depleted.[9] Consistently, CD3e-IT has shown to reliably prolong allograft acceptance but fails to sustain long-term tolerance[12–14]. The efficacy of CD3-immunotoxin may also be dependent upon the route of injection,[9] but how specialized anatomical microenvironments and local lymphoid structures contribute to immunotoxin resistance remains unknown.

The secondary lymphoid follicle contains the germinal center (GC), a specialized microenvironment dedicated to B-cell clonal expansion, somatic hypermutation, and antibody affinity maturation.[15] The GC is recognized as a semi-immune-privileged zone, providing sanctuary for GC-resident T cells, including follicular helper T cells (T_{FH}; $CD4^+CXCR5^+PD\text{-}1^{hi}$) and follicular regulatory T cells (T_{FR}; $CD4^+Foxp3^+CXCR5^+PD\text{-}1^{hi}$).[16] These cells are crucial in orchestrating and fine-tuning these humoral events[17] and have been implicated in autoimmunity and the development of several T-cell lymphomas.[18–23] They are also a key HIV-1 reservoir[16] and are likely the cells-of-origin of angioimmunoblastic T-cell lymphoma (AITL), 20–30% of PTCL-NOS (not otherwise specified), and a small portion of CTCLs and other PTCLs.[18–23] Treating these cells has been particularly challenging; cytotoxic $CD8^+$ T cells are excluded in the GC via chemokine receptor mismatches[16] and drug penetration into lymph node parenchyma has also been shown inefficient.[24–27]

Regarding protein entry into GC, the fibroblastic reticular cell (FRC) conduit network in lymph nodes enforces a strict hydrodynamic filter (~ 70 kDa cutoff), channeling small solutes into follicular parenchyma while excluding larger macromolecules.[28, 29] Nevertheless, intact host and therapeutic immunoglobulins (~ 150 kDa) access the GC through cell-mediated transfer across the subcapsular sinus, ultimately being captured and displayed on follicular dendritic cells (FDCs).[28, 30, 31]

Despite these characterized entry routes, whether other non-immunoglobulin foreign protein agents—such as immunotoxins or other therapeutic protein biologics—can access the GC parenchyma and kill resident follicular T cells has remained unaddressed. Here, using a non-mitogenic CD3-IT with intravascular staining (IVS),[9, 32] we provide a systemic, organ-level analysis of follicular T-cell survival. We demonstrate that the GC microenvironment acts as a macromolecular sanctuary that shields resident $\mathrm{T_{FH}}$ and $\mathrm{T_{FR}}$ cells from circulating immunotoxins (~ 278 kDa) as well as smaller diphtheria toxin molecules (~ 58 kDa). Transient co-stimulatory blockade using an Fc-silent anti-CD40L mAb collapses this structural sanctuary, markedly improving immunotoxin-mediated clearance of the follicular T-cell compartment.

Results

CD3-IT Enables Effective Depletion of Circulating and Tissue-Resident T Cells with Distinct Organ Variations

To dissect the multi-organ depletion kinetics of immunotoxins, C57BL/6J mice were treated with vehicle (PBS), non-depleting isotype immunotoxin (Iso-IT), or an optimized anti-murine CD3 immunotoxin (15 μg

or 25 μg CD3-IT; twice daily for 4 consecutive days) following the previously established protocols (Fig. 1A-i).[9] The CD3-IT conjugate was prepared using a non-mitogenic, Fc-silent anti-CD3 mAb (145-2C11 with Fc-silent™ murine IgG1) coupled to streptavidin-saporin (sZAP) at an optimized 1:1 molar ratio, eliminating unreacted antibody.[32] A control immunotoxin (Iso-IT) was also generated by conjugating isotype-matched antibody with Fc-Silent mutant (Absolute Antibody, Upper Heyford, UK) with sZAP with similar procedures described above. On Day 6, circulating (IVS^+) leukocytes were distinguished from tissue-resident (IVS^-) cells by injecting PE/Cy7-CD45.2 intravenously 3 minutes prior to sacrifice, followed by *ex vivo* labeling with BV650-CD45.2 (Fig. 1A-i).

Administration of 25 μg CD3-IT achieved deep, systemic depletion of $CD3^+$ T cells across both circulating and tissue compartments (Fig. 1A **and Fig. S1A**). In peripheral blood, absolute circulating $CD3^+$ T cells were reduced from 113.33 ± 15.14 cells/μL blood in PBS controls to 4.27 ± 1.37 cells/μL (96.23% depletion; $p < 0.0001$). Within tissue parenchyma (IVS^-), absolute $CD3^+$ counts dropped profoundly: whole spleen resident T cells fell from 3.95 (± 0.57) · 10^6 to 0.30 (± 0.07) · 10^6 (92.29% depletion; $p < 0.0001$), Peyer's patches from 5.84 (± 0.92) · 10^4 to 1.12 (± 0.42) · 10^4 (80.76% depletion; $p = 0.0001$), and mesenteric LNs from 9.28 (± 1.62) · 10^5 to 0.31 (± 0.08) · 10^5 (96.66% depletion; $p < 0.0001$). Peripheral lymph node chains showed similarly high clearance: resident $CD3^+$ T cells in inguinal LNs dropped from 5.05 (± 0.95) · 10^5 to 0.35 (± 0.05) · 10^5 (93.04% depletion; $p = 0.0001$), and mandibular LNs fell from 4.84 (± 0.88) · 10^5 to 0.47 (± 0.14) · 10^5 (90.2% depletion; $p = 0.0003$) (Fig. 1A**-iii and Fig. S1A**). Both $CD4^+$ and $CD8^+$ T-cell subsets were significantly reduced at similar levels in all lymphoid tissues (**Fig. S1A**), with $CD8^+$ T cells exhibiting heightened susceptibility, consistent with prior findings.[9]

Follicular T Helper (T) and Regulatory (T) Cells Are Disproportionately Enriched

Despite extensive overall T-cell clearance, phenotypic analysis of the surviving $CD4^+$ T-cell pool revealed substantial enrichment of follicular T helper cells (T_{FH}) (Fig. 1B). Given inconsistent germinal center formation in mice in specific pathogen-free conditions,[33–35] we initially optimized immunization conditions that induce robust germinal center formation and reproducible detection of $CD4^+CXCR5^+PD\text{-}1^{hi}$ T_{FH} after CD3-IT treatment. We found that a single immunization with ovalbumin (OVA) in complete Freund's adjuvant (CFA) exhibit consistently high $CXCR5^+/CXCR5^-$ $CD4^+$ T-cell ratios inversely correlated with the absolute surviving fraction of total $CD4^+$ T cells (Fig. 1B-i).

Consistently, the frequency of T_{FH} among surviving tissue $CD4^+$ T cells increased in mice that show higher T-cell depletion rates (Fig. 1B**-iii**). T_{FH} frequency significantly rose in the peripheral blood from 0.35 ± 0.08% in PBS-treated mice to 3.83 ± 1.07% in 25 μg CD3-IT-treated mice ($p = 0.0315$) and in the spleen (2.45 ± 0.33% in PBS to 9.48 ± 1.34% in 25 μg CD3-IT; $p = 0.0051$). It also substantially rose across all secondary lymphoid tissues examined, including mesenteric LNs (2.18 ± 0.28% to 8.30 ± 1.34%; $p =$

0.0091), mandibular LNs (1.99 ± 0.27% to 5.36 ± 1.49%; $p = 0.0871$), inguinal LNs (0.94 ± 0.19% to 2.91 ± 0.54%; $p = 0.0191$), lumbar LNs (3.37 ± 0.49% to 10.53 ± 1.89%; $p = 0.0174$), and Peyer's patches (16.99 ± 2.02% to 30.06 ± 7.25%; $p = 0.1476$) (Fig. 1B**-iii**). Consistently, an independent analysis of 15 µg CD3-IT treatment confirmed that both GC-resident follicular regulatory T cells ($CD4^+Foxp3^+CXCR5^+PD\text{-}1^{hi}$ T_{FR}) and T_{FH} ($CD4^+Foxp3^-CXCR5^+PD\text{-}1^{hi}$) were similarly preserved and enriched in all tested organs, except bone marrow (**Fig. S1B**). Bone marrow is known to actively retain T regulatory cells (via CXCL12/CXCR4 signals)[36] and showed unique T-cell composition in both homeostatic conditions and after CD3-IT treatment.[9]

Follicular T Cells Possess No Cell-Intrinsic Resistance to CD3-IT Binding or Cytotoxicity.

To establish whether the selective survival of T_{FH} cells resulted from altered target binding or cellular resistance to saporin catalytic activity, we analyzed primary splenocyte subsets *ex vivo* (Fig. 2). Splenocytes from immunized mice were incubated with 10 nM CD3-IT for 0, 5, 10, 20, 30, or 60 minutes and probed with an anti-saporin mAb (Fig. 2A). CD3-IT bound rapidly to cell-surface CD3 on T cells, peaking at about 5 mins for both $CD4^+$ and $CD8^+$ T cells. At 5 minutes, CD3-IT binding was broadly similar between $CD4^+CXCR5^-$ and $CD4^+CXCR5^+$ subsets (8.9 ± 2.8% vs 10.7 ± 2.7% at 5 min, $p = 0.460$ by Welch's test) (Fig. 2A). $CD8^+$ T cells exhibited lower overall binding, in line with their lower baseline CD3 surface density, but showed no difference between $CXCR5^-$ and $CXCR5^+$ subsets (3.9 ± 1.3% vs 3.2 ± 1.6% at 5 min, $p = 0.607$ by Welch's test) (Fig. 2A).

Next, splenic $CD3^+$ cells (negative selection) were pulsed with escalating concentrations of CD3-IT (0.1, 1.0, and 10.0 nM) for 30 minutes, washed, and cultured under anti-CD3/anti-CD28 co-stimulation for 72 hours (Fig. 2B). CD3-IT induced robust, dose-dependent cytotoxicity across all subsets without significant divergence: cell viability fell to 32.0 ± 1.9% at 1.0 nM and 11.0 ± 2.3% at 10.0 nM in bulk $CD3^+$ T cells, compared to 34.1 ± 1.7% and 11.5 ± 2.2% in $CD3^+CXCR5^+$ T cells, and 26.2 ± 3.7% and 9.7 ± 2.7% in $CD3^+CXCR5^-$ T cells (Fig. 2B). No significant difference in viability was observed between $CXCR5^+$ and $CXCR5^-$ populations at any dose ($p > 0.05$). IC_{50} values between $CXCR5^+$ and $CXCR5^-$ populations (0.569 nM vs. 0.471 nM) were not significantly different ($p > 0.05$). Thus, CXCR5 + follicular T cells possess no cell-intrinsic resistance to CD3-IT binding, internalization, or ribosome-inactivating catalytic death.

Germinal Center Microenvironment Restricts In Vivo Immunotoxin Entry

We next evaluated whether the anatomical architecture of the lymphoid follicle protects resident T cells *in vivo* (Fig. 3). Paraffin-embedded spleen sections from PBS- and CD3-IT-treated mice were stained for CD3, CD20, and peanut agglutinin (PNA) to delineate periarteriolar lymphoid sheath T-cell zones (TZ) and PNA^+ germinal centers (GC) (Fig. 3A). Digital morphometric analysis revealed a profound, selective depletion of T cells within splenic TZs: absolute T-cell numbers plummeted 5.8-fold ($p = 0.0001$) from 915 ± 509.8 cells/field in PBS controls (n = 14) to 158.5 ± 70.6 cells/field in CD3-IT-treated mice (n = 13), representing an 83% loss (Fig. 3A). In contrast, intra-GC T cells showed relatively mild reduction from

62.9 ± 36.2 cells/GC in controls (n = 10) to 33.4 ± 30.6 cells/GC in treated mice (n = 12) (1.9-fold; p = 0.0566) (Fig. 3A). Mean GC cross-sectional area remained unaltered (21,001 ± 17,986 μm^2 vs. 15,633 ± 12,070 μm^2; p = 0.4332), indicating intact GC boundaries (Fig. 3A).

To assess why GC-resident T cells escaped depletion, we examined the relationship between basal CD3 surface density (mean fluorescence intensity, MFI) and *in vivo* depletion across four subsets defined by CXCR5 and PD-1 expression (Fig. 3B). In peripheral blood, spleen, and lymph nodes, extra-follicular populations ($CXCR5^-PD\text{-}1^{neg/dim}$ naive cells, $CXCR5^-PD\text{-}1^{hi}$ effector cells, and $CXCR5^+PD\text{-}1^{neg/dim}$ memory-like T_{FH}) exhibit a linear relationship: higher surface CD3 expression corresponded to higher *in vivo* fold-depletion (Figs. 3B and S2A).[17] In the spleen, $CXCR5^-PD\text{-}1^{neg/dim}$ cells (CD3 MFI: 38,885) exhibited 20.2 ± 5.4-fold reduction, while $CXCR5^+PD\text{-}1^{neg/dim}$ cells (CD3 MFI: 45,599) showed 35.2 ± 4.8-fold reduction. In sharp contrast, germinal center T_{FH} cells (GC-T_{FH}; $CXCR5^+PD\text{-}1^{hi}$) despite expressing high surface CD3 (MFI:45,430), exhibited only 11.5±10.7-fold reduction, departing significantly from the linear regression line established by non-follicular subsets [Figs. 3B**-iii** (25 µg CD3-IT) and **S2A** (15 µg CD3-IT)]. This selective departure was confirmed in mesenteric and mandibular LNs (Figs. 3B**-iii** and **S2A**).

To assess short-term *in vivo* cell-associated CD3-IT binding, mice were injected with 15 µg CD3-IT, followed 5 minutes later by IVS antibody injection and euthanasia at 8 minutes (Fig. 3C-i). This short-term treatment enables CD3-IT to penetrate tissue parenchyma and bind tissue-resident T cells. In circulation (IVS^+), CD3-IT bound with high efficiency to both $CD4^+CXCR5^-$ and $CD4^+CXCR5^+$ T cells (80.3 ± 4.4% vs. 75.4 ± 7.9%; Holm-adjusted $p > 0.05$) and $CD8^+$ T cells (60.7 ± 8.4% vs. 65.0 ± 4.1%; Holm-adjusted $p > 0.05$) (Fig. 3C-i**i**). Within the splenic parenchyma (IVS^-), however, immunotoxin binding to $CD4^+CXCR5^+$ cells were significantly lower than the $CXCR5^-$ counterpart ($CD4^+CXCR5^+$: 8.4 ± 4.9% vs. $CD4^+CXCR5^-$: 14.5 ± 7.6%; Holm-adjusted p = 0.0099) (Fig. 3C-i**ii**). Notably, GC-T_{FH} bound only 7.5 ± 4.8% compared to 15.1 ± 7.8% of non-T_{FH} cells (Holm-adjusted p = 0.0041). Similarly, $CD8^+CXCR5^+$ cells also showed significantly lower binding than the $CXCR5^-$ counterpart ($CD8^+CXCR5^+$: 4.2 ± 2.0% vs. $CD8^+CXCR5^-$: 11.3 ± 6.5%; Holm-adjusted p = 0.0333)

In vivo BrdU incorporation assays revealed that while CD3-IT treatment triggered homeostatic proliferation across surviving T cells (Figs. 3D and S2B) consistent with previous reports,[37] GC-T_{FH} displayed no significant differences compared to extra-follicular subsets (e.g., in spleen: 45.8 ± 6.2% $BrdU^+$ in GC-T_{FH} vs. 35.4 ± 5.1% in $CXCR5^-PD\text{-}1^{hi}$ effector cells at 25 µg CD3-IT). Therefore, T_{FH} persistence reflects physical protection by the GC rather than compensatory hyper-proliferation.

Pre-Treatment with Anti-CD40L Disassembles GCs and Restores T Depletion

Given the organized GC structure limits immunotoxin penetration into GC, we further tested whether pharmacological dissolution of GCs would improve T_{FH} depletion. Mice received a single injection of an Fc-silent anti-CD40L mAb (aCD40L-TM-mAb; 2 mg) 24 hours prior to initiating CD3-IT treatment (Fig. 4B-i). Fc-silent anti-CD40L antibodies can disrupt GC responses without the thromboembolic complications associated with earlier Fc-intact antibodies.[38–40] Serial histology confirmed that aCD40L-TM-mAb administration induced rapid GC involution: splenic GC numbers dropped from 9.3 ± 2.3 at Day 0 to 1.0 ± 1.0 by Day 6 (p = 0.0132, Welch's T test) (Fig. 4A-**ii, iii**). In mesenteric LNs, GCs were undetectable by Day 6 (p = 0.0272) (Fig. 4A-**ii, iii**). In contrast, T-cell zone areas and baseline T-cell densities remained largely unperturbed (Fig. 4A-v, **vi**). Anti-CD40L pre-treatment caused no additional weight loss or overt clinical toxicity beyond CD3-IT monotherapy (Fig. 4B-**ii**).

Dissolving GCs with CD40L blockade effectively reduced T_{FH} cells in all tested organs (Figs. 4C and S3). While CD3-IT monotherapy substantially increased the surviving splenic T_{FH} fraction to be 2.944 ± 1.792% (15 μg) and 5.823 ± 1.253% (25 μg) of $CD4^+$ T cells, pre-treatment with anti-CD40L prior to CD3-IT (combination therapy) significantly reduced the T_{FH} proportion to 0.008 ± 0.008% of $CD4^+$ T cells (776.4-fold reduction, p = 0.0188 vs. 25 μg CD3-IT alone) (Fig. 4C). Mesenteric LNs showed notable reduction: from 3.139 ± 0.924% (25 μg) to 0.273 ± 0.082% (11.5-fold reduction, p = 0.0526). In the peripheral blood, combination treatment also reduced the surviving T_{FH} fraction from 1.998 ± 0.627% to 0.233 ± 0.233% (8.6-fold reduction, p = 0.0645) (**Fig. S3**).

In contrast to the inefficient GC-T_{FH}-cell depletion with single 15 μg CD3-IT treatment, departing significantly from the linear regression line between T-cell reduction rates and surface CD3 expression levels established by non-follicular subsets (Fig. 4D, **upper panel**), the combination treatment (aCD40L-TM-mAb + CD3-IT) showed increased depletion rates of GC-T_{FH} cells that realigned with the predicted linear depletion trajectory in the tissue parenchyma (ISV^-), matching the clearance kinetics of non-follicular T cells (Fig. 4D, **lower panel**).

Germinal Centers Enforce Selective Macromolecular Gatekeeping Against Foreign Toxins and Toxin-Conjugates.

The fibroblastic reticular cell (FRC) conduit network in secondary lymphoid tissues enforces a size-exclusion boundary, permitting passive diffusion of small soluble molecules (< 70 kDa) into interfollicular regions while excluding larger globular entities. However, intact immunoglobulins (~ 150 kDa) readily access follicular parenchyma, mediated by interstitial percolation and retention on follicular dendritic cell (FDC) networks. To determine whether follicular sanctuary is governed strictly by molecular weight cutoffs or by molecular identity, we evaluated CD4-iDTR mice—which express the diphtheria toxin receptor on $CD3^+$ T cells (both $CD4^+$ and $CD8^+$) (Fig. 5A-i)—challenged with diphtheria toxin (DT; ~58 kDa), bulky CD3-IT conjugates (~ 278 kDa), and Fc-silent CD3 mAbs (~ 150 kDa; 145-2C11 with Fc-silent™ murine IgG1).

Consistent with previous reports, systemic administration of free DT (200 ng twice daily for 4 days) resulted in profound T-cell depletion, as well as body-/organ-weight changes, comparable to CD3-IT (Figs. 5A-C and S4A-D). In the spleen, DT ablated T cells within interfollicular TZs (17.9-fold reduction; $p < 0.0001$; 1066.7 ± 498.9 cells in PBS controls to 59.5 ± 48.1 cells in DT mice) (Fig. 5D). However, intra-GC T cells remained relatively less depleted (3.7-fold reduction; $p = 0.0013$; 16.5 ± 11.5 cells/GC in controls vs. 4.5 ± 3.5 cells/GC in DT-treated mice) (Fig. 5D). Flow cytometry confirmed that DT treatment caused a marked enrichment of $CXCR5^{+}PD\text{-}1^{hi}$ T_{FH} cells across the spleen (2.0-fold increase; $p = 0.0167$), mesenteric LNs (1.9-fold increase; $p = 0.0423$), and Peyer's patches (2.2-fold increase; $p = 0.0098$), mirroring CD3-IT (Figs. 5E and S4E). Given relatively small size of free DT (~ 58 kDa), which is below the canonical 70 kDa conduit size-exclusion boundary, protein size exclusion alone cannot explain this T_{FH} cell enrichment.

In contrast, treatment with unconjugated Fc-silent CD3-mAb (~ 150 kDa) induced near-complete surface CD3 modulation across both $CD4^{+}$ and $CD8^{+}$ T cells without causing cell death (Figs. 5B-C **and Fig. S4F**). Notably, CD3-mAb treatment did not show any notable enrichment of T_{FH} cells within CD3 + CD4+ T cell population in any lymph-node chain (Figs. 5E and S4E). The ability of unconjugated CD3 mAb (~ 150 kDa) to induce CD3 down-modulation on GC-T_{FH} is consistent with antibody engagement in or near the GC; however, our experiments do not resolve whether this reflects direct intrafollicular penetration[28, 30, 31] or engagement of T_{FH} cells that transiently exit the GC.[17] In contrast, the failure of both free DT (~ 58 kDa) and CD3-IT conjugate (~ 278 kDa) to deplete GC-resident cells, coupled with restoration of depletion after GC disruption, identifies intact GC architecture as the principal barrier to functional toxin delivery.

Together, these findings indicate that intact GC architecture creates a functional barrier to toxin-mediated depletion of resident follicular T cells.

Discussion

Understanding why targeted biologics fail to achieve complete eradication of target-cell populations is essential for improving immunotoxin therapy in transplantation and oncology. Our findings identify the germinal center (GC) of B-cell follicles as an anatomical and functional sanctuary that protects follicular helper (T_{FH}) and regulatory (T_{FR}) T cells from CD3 immunotoxin (CD3-IT)–mediated depletion. Although CD3-IT achieved > 93–99% depletion of circulating and interfollicular T cells, GC-resident T cells persisted and became enriched within the surviving CD4 + compartment.

Ex vivo binding and killing assays showed that CXCR5 + T cells bound CD3-IT and remained fully susceptible to saporin-mediated cytotoxicity (IC_{50} = 0.471 nM). Thus, their *in vivo* survival is not readily explained by intrinsic resistance to CD3-IT. Rather, the data support limited productive delivery of toxin to cells within the intact GC microenvironment. The fibroblastic reticular cell conduit system imposes a size-selective route for lymph-borne solutes, but its approximately 70-kDa cutoff applies to conduit-

mediated transport and cannot alone explain access to the B-cell follicle or GC.[28, 29] Notably, free diphtheria toxin (~ 58 kDa) failed to deplete intra-GC T cells in vivo and enriched TFH cells similar to the ~ 278-kDa CD3-IT conjugate. These findings indicate that molecular size alone does not determine effective toxin delivery to GC-resident cells.

Conversely, unconjugated Fc-silent anti-CD3 mAbs induced CD3 down-modulation on GC-TFH cells, demonstrating that these cells can be exposed to anti-CD3 mAb *in vivo*. However, this observation does not by itself establish uniform penetration of soluble mAb throughout the GC. CD3 engagement could occur within or near the GC (potentially through direct intrafollicular penetration) or during the dynamic trafficking of follicular T cells at the GC boundary and outside the follicle.[17] Thus, the mAb results are compatible with access to follicular T cells,[25, 27] while remaining compatible with insufficient GC exposure to intact toxins or toxin-containing conjugates. Our studies do not distinguish absolute exclusion of toxin from reduced local exposure, retention, or productive intracellular delivery within the GC microenvironment.

Short half-life of immunotoxins[1, 41] may further limit its access to the GC. Conjugation to streptavidin-saporin can alter the pharmacokinetics of the anti-CD3 mAb, and uptake by CD3 + T cells and other tissues may shorten the period during which intact CD3-IT remains available in circulation. This limited exposure may compound the GC barrier, although CD3-IT pharmacokinetics and intra-GC concentrations were not measured in this study.

This sanctuary has direct clinical and therapeutic implications. In solid-organ and vascularized composite allotransplantation, CD3-IT conditioning can support durable mixed chimerism yet may not produce complete operational tolerance, with late humoral rejection driven by donor-specific antibodies.[4, 5, 14] Persistence of GC-T_{FH} and T_{FR} cells provides a potential mechanistic explanation because these cells support B-cell selection, somatic hypermutation, and alloantibody production. [42–44] Similarly, in peripheral T-cell lymphomas with T_{FH} features, including angioimmunoblastic T-cell lymphoma,[18, 19] the GC microenvironment may provide a protected niche for malignant cells.

The finding that brief pretreatment with Fc-silent anti-CD40L mAb disrupts GC architecture and substantially restores CD3-dependent depletion of T_{FH} cells provides an actionable translational strategy. Recent studies showed Fc-silenced or Fc-deleted CD40L-targeting agents[38–40] can disrupt GC responses without the thromboembolic complications associated with earlier CD40L antibodies.[45–48] CD40L blockades, an important immune-inflammatory modulator,[45–48] may also reduce immunotoxin-treatment-associated immune responses.[49]

These results support a model in which transient modulation of the follicular microenvironment can expose a protected cellular reservoir to CD3-IT. Although increasing CD3-IT dose or duration could potentially improve local exposure, this approach may be constrained by systemic toxicity, including

vascular leak syndrome. Combining targeted immunotoxins with transient GC-modulating biologics may therefore offer a more rational path toward deeper depletion of protected follicular T-cell reservoirs.

Methodology

Animals and In Vivo Treatments

All animal studies were conducted in accordance with the National Institutes of Health Guide for the Care and Use of Laboratory Animals and were approved by The Ohio State University Institutional Animal Care and Use Committee (IACUC; protocol 2016A00000020-R3). Work involving biohazardous materials was conducted under oversight of The Ohio State University Institutional Biosafety Committee (IBC; protocol 2016R00000009-R2).

Male C57BL/6J (4–6 months old) and CD4-iDTR mice (> 6 months old) were bred and housed under specific pathogen-free conditions in accordance with protocols approved by the Institutional Animal Care and Use Committee (IACUC) at The Ohio State University (Protocol #2016A00000020). CD4-iDTR mice were generated by crossing B6.Cg-Tg(CD4-cre)1Cwi/BfluJ (Jax #017336) with C57BL/6-Gt(ROSA)26Sor$^{tm1(HBEGF)Awai}$/J (Jax #007900), and verified by genomic PCR as described previously.[32, 50]

Germinal centers were induced by intraperitoneal injection of 100 µg ovalbumin (OVA; Sigma-Aldrich) emulsified 1:1 in complete Freund's adjuvant (CFA; Sigma-Aldrich). For mice receiving a booster, 100 µg OVA in incomplete Freund's adjuvant (IFA; Sigma-Aldrich) was injected at one, three or four weeks after the initial OVA/CFA injection. Two weeks post-initial immunization, mice received retro-orbital injections twice daily for 4 consecutive days of sterile PBS, non-depleting isotype immunotoxin (Iso-IT; 15 µg), CD3-IT (15 or 25 µg), or diphtheria toxin (DT; 200 ng; Sigma-Aldrich). For GC-dissolution experiments, mice received a single retro-orbital dose of 2 mg Fc-silent anti-CD40L mAb (clone MR-1 with murine IgG1 Fc-silent mutations; Absolute Antibody) 24 hours prior to initiating CD3-IT. For proliferation assays, mice received 100 µg BrdU (BD Biosciences) intraperitoneally 24 hours prior to sacrifice.

Preparation of Immunotoxins and Antibodies

Fc-silent chimeric anti-mouse CD3 mAb (clone 145-2C11 with murine IgG1 Fc-silent mutations) and Fc-silent isotype controls were purchased from Absolute Antibody. Monoclonal antibodies were biotinylated using the FluoReporter Mini-Biotin-XX Protein Labeling Kit (Invitrogen) at an optimized ratio of 4 µL biotin solution per 1 mg antibody (1 mg/mL). Biotinylated antibodies were conjugated to streptavidin-saporin (sZAP; Advanced Targeting Systems) at a 1:1 molar ratio in a 4°C walk-in cold room to eliminate unreacted free antibody. Intact hamster anti-CD3 (145-2C11; Bio X Cell) was used as a mitogenic antibody control.

Intravascular Staining and Tissue Processing

Circulating and tissue-resident leukocytes were distinguished by retro-orbital injection of 3 µg PE/Cy7-CD45.2 (clone 104; BioLegend) in 200 µL sterile DPBS 3 minutes prior to euthanasia. Peripheral blood was collected via cardiac puncture into EDTA tubes. Spleen, Peyer's patches, thymus, bone marrow (femur), and five lymph node chains (mesenteric, inguinal, mandibular, mediastinal, and lumbar) were dissected and dissociated through 70 µm nylon cell strainers into ice-cold RPMI-1640. Red blood cells were lysed with ACK lysis buffer (Gibco).

Flow Cytometry and Functional Assays

Single-cell suspensions were blocked with TruStain FcX (anti-mouse CD16/32; BioLegend) and stained with Zombie Aqua Fixable Viability Kit (BioLegend). Surface staining was performed using fluorochrome-conjugated antibodies against CD45.2 (BV650; 104), CD3 (Alexa Fluor 700; 500A2), CD4 (Pacific Blue; RM4-5), CD8 (BV570; 53 – 6.7), CD19 (BV711; 6D5), CD44 (PerCP/Cy5.5; IM7), CD62L (APC/Cy7; MEL-14), CXCR5 (Alexa Fluor 647; L138D7), and PD-1 (BV421; RMP1-30). Intracellular Foxp3 was detected using the Foxp3/Transcription Factor Staining Buffer Set (Invitrogen) and PE/Cy5-Foxp3 (FJK-16s). BrdU incorporation was measured using the APC BrdU Flow Kit (BD Biosciences). Absolute cell counts were quantified using CountBright Absolute Counting Beads (Invitrogen) on a Cytek Aurora spectral cytometer and analyzed using FlowJo software (BD Biosciences).

For *ex vivo* binding, splenocytes ($1.5 \cdot 10^6$ cells) were pulsed with 10 nM CD3-IT in complete RPMI-1640 at 37°C for 0, 5, 10, 20, 30, or 60 minutes, washed twice in cold PBS containing 2% FBS, and labeled with anti-saporin mAb (Advanced Targeting Systems) followed by flow cytometric analysis. For *ex vivo* cytotoxicity, total splenic CD3 + T cells were isolated by negative selection using MojoSort (BioLegend), incubated with CD3-IT (0, 0.1, 1.0, or 10.0 nM) for 30 minutes, washed, and cultured with anti-CD3/anti-CD28 stimulation. Viability of bulk CD3+, CD3 + CXCR5+, and CD3 + CXCR5− subsets was measured by flow cytometry after 72 hours. For *in vivo* short-term binding, mice received 15 µg CD3-IT or Iso-IT retro-orbitally, followed 5 minutes later by PE/Cy7-CD45.2 IVS injection and sacrifice 3 minutes later (8 minutes total exposure), with isolated cells stained *ex vivo* with anti-saporin mAb.

Immunohistochemistry and Morphometry

Tissue specimens were fixed in 10% neutral-buffered formalin, embedded in paraffin, sectioned at 4 µm, and stained with H&E, anti-CD3 (Dako), anti-CD20 (eBioscience), and biotinylated peanut agglutinin (PNA; Vector Laboratories). Digital imaging was performed by HistoWiz. Morphometric areas (μm^2) and intra-zonal T-cell numbers across splenic T-cell zones and germinal centers were quantified using cellSens software across 10–15 distinct follicles per animal in a blinded manner.

Statistical Analysis

Data represent mean ± SEM unless indicated otherwise. All dose-response curves, nonlinear regressions, and statistical tests were performed using GraphPad Prism and R. Cell viability percentages were

normalized against baseline PBS controls within each experimental batch. To calculate IC50 values, log-transformed molar concentrations were fitted to a four-parameter variable-slope sigmoidal dose-response model [Y = Bottom + (Top - Bottom) / (1 + $10^{(LogIC50-X)xHillSlop}$)]. The upper plateau (Top) was constrained to 100% and the lower plateau (Bottom) was constrained to 0%. Differences in IC50 parameters between $CXCR5^-$ and $CXCR5^+$ subsets were evaluated by extra sum-of-squares F-tests comparing individual vs. shared parameter models. A p-value < 0.05 was considered statistically significant. Statistical comparisons between two groups were evaluated using two-tailed Welch's t-tests or Mann-Whitney U tests. Significance is indicated as * $p < 0.05$ and ** $p < 0.01$.

References

1. Frankel AE et al (2015) Resimmune, an anti-CD3ε recombinant immunotoxin, induces durable remissions in patients with cutaneous T-cell lymphoma. Haematologica 100:794
2. Foss FM et al (2025) Efficacy and Safety of Denileukin Diftitox-Cxdl, an Improved Purity Formulation of Denileukin Diftitox, in Patients With Relapsed or Refractory Cutaneous T-Cell Lymphoma. J Clin Oncol 43:1198–1209
3. Jonker M et al (2002) Long-term kidney graft survival by delayed T cell ablative treatment in rhesus monkeys. Transplantation 73:874–880
4. Leonard DA et al (2014) Vascularized composite allograft tolerance across MHC barriers in a large animal model. Am J Transpl 14:343–355
5. Huang CA et al (2000) Stable mixed chimerism and tolerance using a nonmyeloablative preparative regimen in a large-animal model. J Clin Invest 105:173–181
6. Hu H et al (1997) Depletion of T lymphocytes with immunotoxin retards the progress of experimental allergic encephalomyelitis in rhesus monkeys. Cell Immunol 177:26–34
7. Wamala I et al (2013) Recombinant anti-monkey CD3 immunotoxin depletes peripheral lymph node T lymphocytes more effectively than rabbit anti-thymocyte globulin in naïve baboons. Transpl Immunol 29:60–63
8. Watanabe R et al (2015) Human skin is protected by four functionally and phenotypically discrete populations of resident and recirculating memory T cells. Sci Transl Med 7:279ra239
9. Kim S et al (2022) CD3e-immunotoxin spares CD62L(lo) Tregs and reshapes organ-specific T-cell composition by preferentially depleting CD3e(hi) T cells. Front Immunol 13:1011190
10. Ermann J et al (2005) Only the CD62L+ subpopulation of CD4 + CD25+ regulatory T cells protects from lethal acute GVHD. Blood 105:2220–2226
11. Taylor PA et al (2004) L-Selectin(hi) but not the L-selectin(lo) CD4 + 25+ T-regulatory cells are potent inhibitors of GVHD and BM graft rejection. Blood 104:3804–3812
12. Torrealba JR et al (2004) Metastable tolerance to rhesus monkey renal transplants is correlated with allograft TGF-beta 1 + CD4+ T regulatory cell infiltrates. J Immunol 172:5753–5764
13. Knechtle SJ et al (1997) FN18-CRM9 immunotoxin promotes tolerance in primate renal allografts. Transplantation 63:1–6

14. Page EK et al (2012) Enhanced de novo alloantibody and antibody-mediated injury in rhesus macaques. Am J Transpl 12:2395–2405
15. Victora GD, Nussenzweig MC (2022) Germinal Centers. Annu Rev Immunol 40:413–442
16. Fukazawa Y et al (2015) B cell follicle sanctuary permits persistent productive simian immunodeficiency virus infection in elite controllers. Nat Med 21:132
17. Crotty S, Follicular Helper (2011) CD4 T Cells (TFH). Annu Rev Immunol 29:621–663
18. de Leval L et al (2007) The gene expression profile of nodal peripheral T-cell lymphoma demonstrates a molecular link between angioimmunoblastic T-cell lymphoma (AITL) and follicular helper T (TFH) cells. Blood 109:4952
19. Ahearne MJ, Allchin RL, Fox CP, Wagner SD (2014) Follicular helper T-cells: expanding roles in T-cell lymphoma and targets for treatment. Br J Haematol 166:326–335
20. Huang Y et al (2009) Peripheral T-cell lymphomas with a follicular growth pattern are derived from follicular helper T cells (TFH) and may show overlapping features with angioimmunoblastic T-cell lymphomas. Am J Surg Pathol 33:682–690
21. Moroch J et al (2012) Follicular peripheral T-cell lymphoma expands the spectrum of classical Hodgkin lymphoma mimics. Am J Surg Pathol 36:1636–1646
22. Bosisio FM, Cerroni L (2015) Expression of T-Follicular Helper Markers in Sequential Biopsies of Progressive Mycosis Fungoides and Other Primary Cutaneous T-Cell Lymphomas. Am J Dermatopathol 37
23. Nicolae A et al (2013) Peripheral T-cell lymphomas of follicular T-helper cell derivation with Hodgkin/Reed-Sternberg cells of B-cell lineage: both EBV-positive and EBV-negative variants exist. Am J Surg Pathol 37:816–826
24. Fletcher CV et al (2014) Persistent HIV-1 replication is associated with lower antiretroviral drug concentrations in lymphatic tissues. *Proceedings of the National Academy of Sciences* 111, 2307
25. Wu F, Tamhane M, Morris ME, Pharmacokinetics (2012) Lymph Node Uptake, and Mechanistic PK Model of Near-Infrared Dye-Labeled Bevacizumab After IV and SC Administration in Mice. AAPS J 14:252–261
26. Pereira ER, Jones D, Jung K, Padera TP (2015) The lymph node microenvironment and its role in the progression of metastatic cancer. Semin Cell Dev Biol 38:98–105
27. Mihalj M, Kellermayer Z, Balogh P (2013) Follicles in gut-associated lymphoid tissues create preferential survival niches for follicular Th cells escaping Thy-1-specific depletion in mice. Int Immunol 25:423–435
28. Roozendaal R et al (2009) Conduits mediate transport of low-molecular-weight antigen to lymph node follicles. Immunity 30:264–276
29. Gretz JE, Norbury CC, Anderson AO, Proudfoot AE, Shaw S (2000) Lymph-borne chemokines and other low molecular weight molecules reach high endothelial venules via specialized conduits while

a functional barrier limits access to the lymphocyte microenvironments in lymph node cortex. J Exp Med 192:1425–1440

30. Phan TG, Green JA, Gray EE, Xu Y, Cyster JG (2009) Immune complex relay by subcapsular sinus macrophages and noncognate B cells drives antibody affinity maturation. Nat Immunol 10:786–793
31. Heesters BA et al (2013) Endocytosis and recycling of immune complexes by follicular dendritic cells enhances B cell antigen binding and activation. Immunity 38:1164–1175
32. Kim S et al (2022) Comparison of CD3e Antibody and CD3e-sZAP Immunotoxin Treatment in Mice Identifies sZAP as the Main Driver of Vascular Leakage. Biomedicines 10:1221
33. Luzina IG et al (2001) Spontaneous formation of germinal centers in autoimmune mice. J Leukoc Biol 70:578–584
34. Poudrier J et al (2001) The AIDS disease of CD4C/HIV transgenic mice shows impaired germinal centers and autoantibodies and develops in the absence of IFN-gamma and IL-6. Immunity 15:173–185
35. Schrock DC et al (2019) Pivotal role for α(V) integrins in sustained Tfh support of the germinal center response for long-lived plasma cell generation. Proc Natl Acad Sci U S A 116:4462–4470
36. Zou L et al (2004) Bone marrow is a reservoir for CD4 + CD25+ regulatory T cells that traffic through CXCL12/CXCR4 signals. Cancer Res 64:8451–8455
37. Page E, Kwun J, Oh B, Knechtle S (2013) Lymphodepletional strategies in transplantation. Cold Spring Harb Perspect Med 3
38. Shock A et al (2015) CDP7657, an anti-CD40L antibody lacking an Fc domain, inhibits CD40L-dependent immune responses without thrombotic complications: an in vivo study. Arthritis Res Ther 17:234–234
39. Yusuf I et al (2014) Germinal center B cell depletion diminishes CD4 + follicular T helper cells in autoimmune mice. PLoS ONE 9:e102791
40. Karnell JL et al (2019) A CD40L-targeting protein reduces autoantibodies and improves disease activity in patients with autoimmunity. Sci Transl Med 11:eaar6584
41. Guo R et al (2016) Fusion of an albumin-binding domain extends the half-life of immunotoxins. Int J Pharm 511:538–549
42. Linterman MA et al (2011) Foxp3 + follicular regulatory T cells control the germinal center response. Nat Med 17:975–982
43. Vaeth M et al (2014) Follicular regulatory T cells control humoral autoimmunity via NFAT2-regulated CXCR5 expression. J Exp Med 211:545–561
44. Crotty ST, Follicular Helper (2019) Cell Biology: A Decade of Discovery and Diseases. Immunity 50:1132–1148
45. Bankert KC et al (2015) Induction of an Altered CD40 Signaling Complex by an Antagonistic Human Monoclonal Antibody to CD40. J Immunol 194:4319

46. Sidiropoulos PI, Boumpas DT (2004) Lessons learned from anti-CD40L treatment in systemic lupus erythematosus patients. Lupus 13:391–397
47. Kim EJ et al (2014) Costimulation blockade alters germinal center responses and prevents antibody-mediated rejection. Am J Transpl 14:59–69
48. Tamada K et al (2002) Blockade of LIGHT/LTβ and CD40 signaling induces allospecific T cell anergy, preventing graft-versus-host disease. J Clin Investig 109:549–557
49. Mazor R, King EM, Pastan I (2018) Strategies to Reduce the Immunogenicity of Recombinant Immunotoxins. Am J Pathol 188:1736–1743
50. Buch T et al (2005) A Cre-inducible diphtheria toxin receptor mediates cell lineage ablation after toxin administration. Nat Meth 2:419–426

Figures

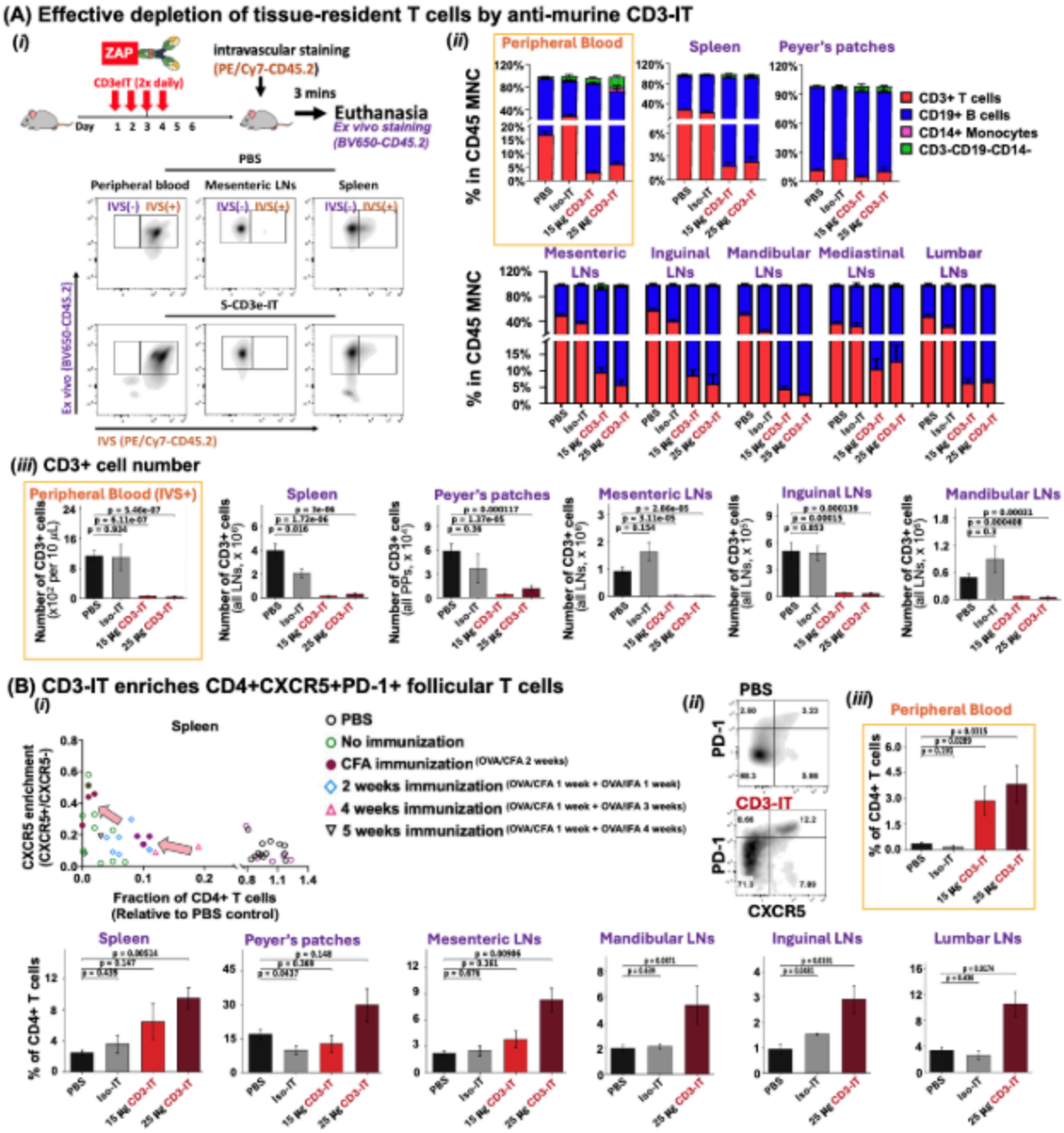


Figure 1

Systemic T-cell depletion by anti-murine CD3epsilon immunotoxin enriches follicular helper (T_{FH}) T cells. (A) Experimental schematic and tissue-resident T-cell depletion: *(i)* Schedule of CD3-IT treatment and intravascular staining (IVS). C57BL/6J mice received retro-orbital injections of vehicle (PBS), non-depleting isotype immunotoxin (Iso-IT), or CD3-IT (15 mg or 25 mg twice daily for 4 consecutive days). On Day 6, mice received PE/Cy7-CD45.2 intravenously 3 minutes prior to sacrifice, followed by *ex vivo* labeling of isolated cells with BV650-CD45.2. Representative flow cytometry plots show segregation of circulating (IVS^+) and tissue-resident (IVS^-) leukocytes in peripheral blood, mesenteric lymph nodes (LNs), and spleen. *(ii)* Proportions of $CD3^+$ T cells, $CD19^+$ B cells, $CD14^+$ monocytes, and $CD3^-CD19^-CD14^-$ null cells among total $CD45^+$ mononuclear cells across indicated organs (n = 3 – 6 mice per

treatment group per organ). *(iii)* Absolute numbers of $CD3^+$ T cells in peripheral blood (IVS^+) and tissue-resident (IVS^-) compartments of the spleen, Peyer's patches, mesenteric LNs, inguinal LNs, and lumbar LNs (n = 9 - 21 for PBS, n = 3 for Iso-IT, n = 9 - 20 for 15 mg CD3-IT, n = 6 for 25 mg CD3-IT). Absolute cell counts were quantified using CountBright beads. **(B) Selective enrichment of $CD4^+CXCR5^+PD\text{-}1^{hi}$ T_{FH} cells:** *(i)* Spleen CXCR5 enrichment ratio ($CXCR5^+/CXCR5^-$) plotted against surviving $CD4^+$ T-cell fractions across non-immunized (n = 12), immunized with single OVA/CFA (n=8). For mice receiving a booster immunization, OVA in incomplete Freund's adjuvant (IFA) was injected 1 week (n = 7), 3 weeks (n = 2), or 4 weeks (n = 1) after the initial OVA/CFA. Inverse correlation between surviving $CD4^+$ T-cell fractions (relative to PBS controls) and $CXCR5^+/CXCR5^-$ ratios. *(ii)* Flow cytometry gating strategy $CD4^+CXCR5^+PD\text{-}1^{hi}$ T_{FH} cells. *(iii)* Percentage of T_{FH} cells among surviving tissue $CD4^+$ T cells across indicated tissues (n = 4-6 for PBS, n = 3 for Iso-IT, n = 5 for CD3-IT).

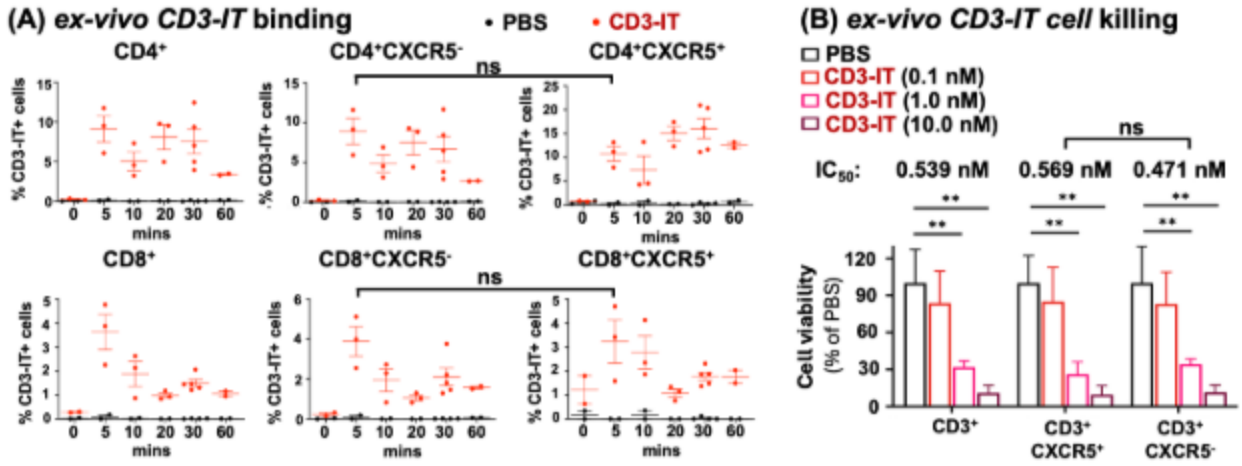


Figure 2

Follicular T cells display no cell-intrinsic resistance to CD3-IT surface binding or catalytic killing *ex vivo*. (A) *Ex vivo* CD3-IT surface binding kinetics: Splenocytes isolated from OVA-immunized C57BL/6J mice were pulsed with 10 nM CD3-IT (red) or vehicle PBS (black) at 37°C for 0, 5, 10, 20, 30, and 60 minutes. Cells were washed, labeled with anti-saporin mAb, and analyzed by spectral flow cytometry. Graphs show the percentage of CD3-IT (saporin)-positive cells over time among total $CD4^+$ T cells, $CD4^+CXCR5^-$, $CD4^+CXCR5^+$ T cells (top panels), and corresponding $CD8^+$ T-cell subsets (bottom panels). % CD3-IT binding between $CXCR5^-$ vs $CXCR5^+$ cells was compared at 5 minutes (p = 0.460 for $CD4^+$ cells; p = 0.607 for $CD8^+$ cells; n=3; Welch's T test). **(B) *Ex vivo* catalytic cell killing assays:** Magnetic-bead-purified bulk $CD3^+$ splenic T cells were pulsed for 30 minutes with escalating concentrations of CD3-IT (0, 0.1, 1.0, and 10.0 nM), washed thoroughly, and cultured in 96-well flat-bottom plates coated with anti-CD3 (5 mg/mL) and soluble anti-CD28 (2 mg/mL). Cell viability was determined by flow cytometry at 72 hours and normalized to untreated (PBS) controls (n = 7). Data represent mean ± SEM. Absolute half-maximal inhibitory concentration (IC_{50}) values were calculated by fitting log(CD3-IT) vs. normalized response curves using a four-parameter logistic (4PL) variable-slope non-linear regression model with

plateaus constrained to 0% (Bottom) and 100% (Top). Best-fit IC_{50} values did not significantly differ between $CXCR5^+$ and $CXCR5^-$ subsets as determined by the extra sum-of-squares F-test (CD3+: $F_{(1,66)}$ = 0.0006, p = 0.981). ** $p < 0.0001$, ns = not significant ($p > 0.05$).

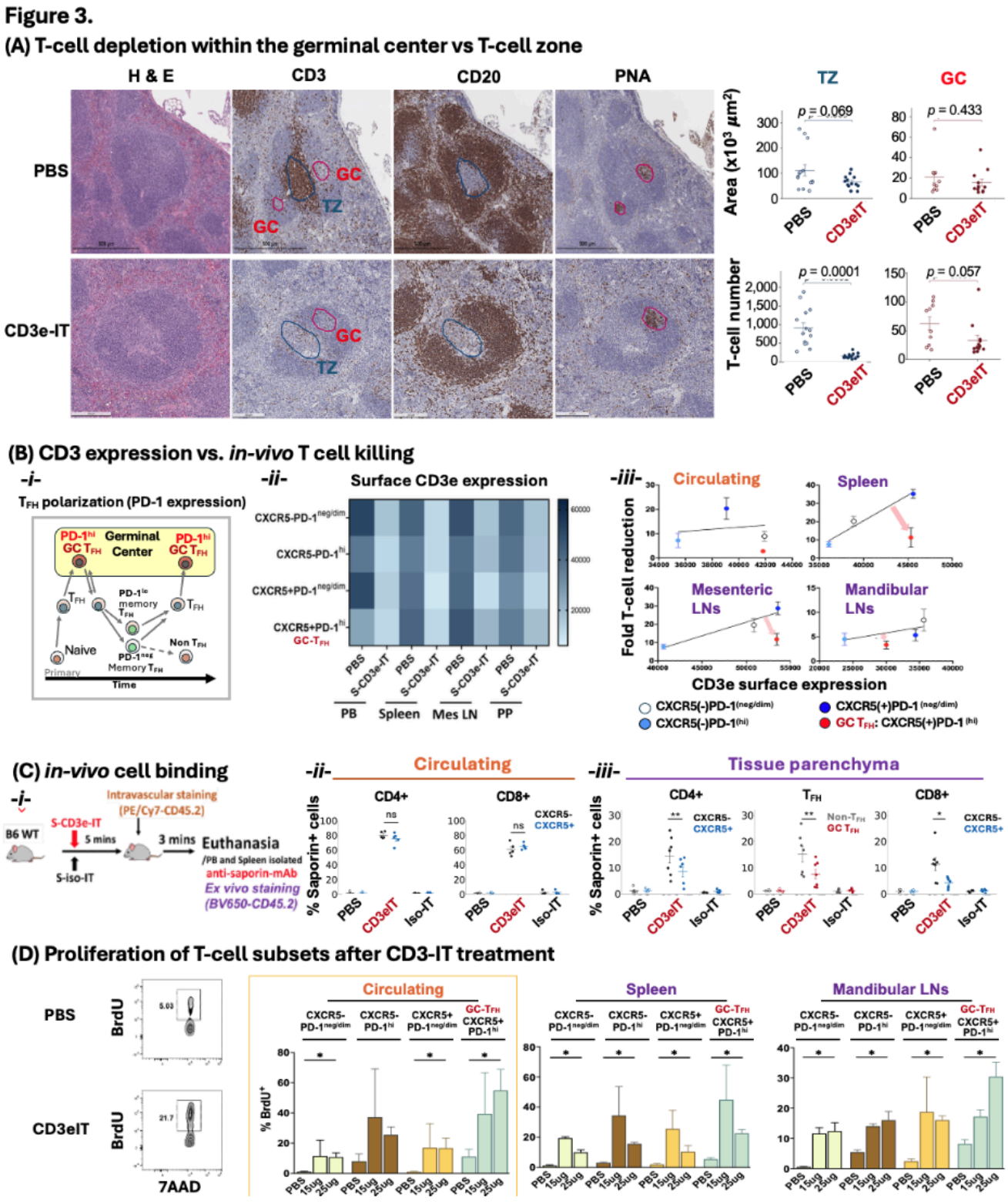


Figure 3

The lymphoid germinal center restricts *in vivo* immunotoxin penetration and protects resident T_{FH} cells. **(A) Splenic microdomain T-cell ablation:** Serial spleen sections from PBS- and CD3-IT-treated mice stained with H&E, anti-CD3 (T cells), anti-CD20 (B cells), and peanut agglutinin (PNA; germinal centers). Blue dashed perimeters mark T-cell zones (TZ); red dashed lines delineate germinal centers (GC). Scale bars = 500 mm. Right scatter plots show total area (mm^2 x 10^3) and absolute T-cell numbers per microscopic field in TZs (n = 14 microscopic fields for PBS; n = 13 microscopic fields for CD3-IT) and GCs (n = 10 GCs for PBS; n = 12 GCs for CD3-IT). Two-sided Welch's t-tests; exact *p*-values are shown. **(B) Correlation of basal CD3epsilon surface density with *in vivo* cell depletion:** *(i)* Polarization schematic of T_{FH} maturation based on CXCR5 and PD-1 expression. *(ii)* Heatmap of basal CD3epsilon mean fluorescence intensity (MFI) across indicated subsets in untreated PBS controls (n = 6 mice for PB, spleen, and mesenteric LNs; n = 4 mice for mandibular LNs). *(iii)* Basal CD3epsilon MFI (x-axis) plotted against *in vivo* fold-depletion [y-axis; 25 mg CD3-IT-treated mice per tissue(n = 4 - 5)] across peripheral blood, spleen, mesenteric LNs, and mandibular LNs. Blue circles indicate extra-follicular subsets adhering to a linear regression slope; red markers denote germinal center T_{FH} cells (GC-T_{FH}; $CXCR5^+PD\text{-}1^{hi}$) departing from the linear trend. **(C) *In vivo* short-term macromolecular binding assay:** *(i)* Workflow: C57BL/6J mice received a single retro-orbital injection of 15 mg CD3-IT or Iso-IT, followed 5 minutes later by PE/Cy7-CD45.2 IVS and euthanasia at 8 minutes. *(ii)* Percentage of saporin-positive cells among circulating (IVS^+) $CD4^+$ and $CD8^+$ T cells (n = 4 mice for PBS; n = 5 mice for CD3-IT; n = 5 mice for Iso-IT). *(iii)* Percentage of saporin-positive cells in tissue-resident (IVS^-) splenic compartments (n = 5 mice for PBS; n = 7 mice for CD3-IT; n = 6 mice for Iso-IT), comparing $CXCR5^-$ vs. $CXCR5^+$ T cells, and non-T_{FH} vs. GC-T_{FH} cells. Two-sided paired t-tests, adjusted across the five comparisons with Holm's method; *$p < 0.05$, ** $p < 0.01$ (circulating $CD4^+$ and $CD8^+$, $p = 0.241$ each; tissue $CD4^+$, $p = 0.00986$; tissue non-T_{FH} versus GC-T_{FH}, $p = 0.00411$; tissue $CD8^+$, $p = 0.0333$.) **(D) *In vivo* proliferation kinetics:** Mice received 1 mg BrdU intraperitoneally 24 hours prior to sacrifice. Representative flow plots (BrdU vs. 7-AAD) and summary bar graphs depict % $BrdU^+$ cells among indicated T-cell subsets in peripheral blood, spleen, and mandibular LNs after PBS (n = 4), 15 mg CD3-IT (n = 4), or 25 mg CD3-IT (n = 4) treatment (* $p < 0.05$).

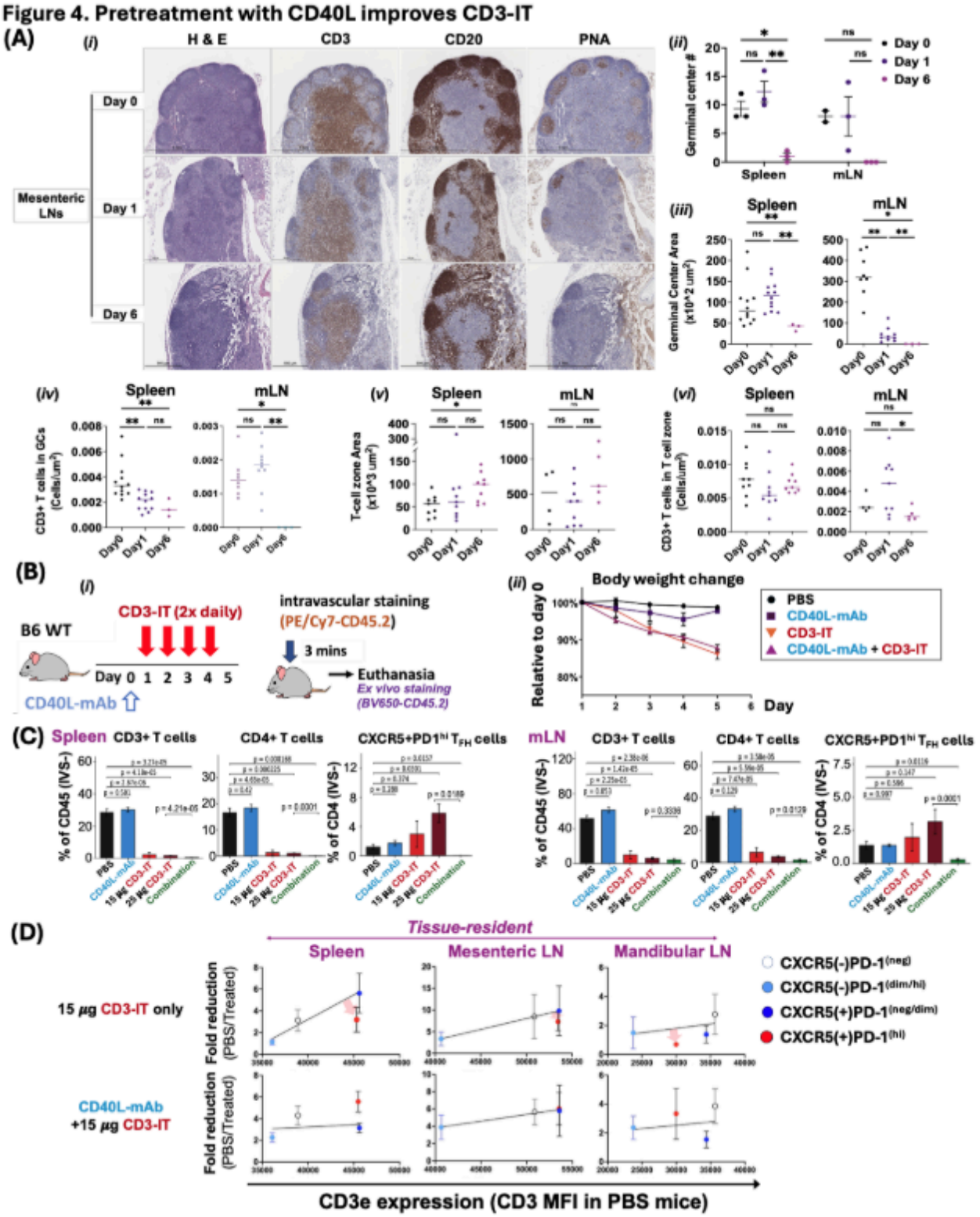


Figure 4

Pre-treatment with Fc-silent anti-CD40L mAb disassembles germinal centers and restores immunotoxin-mediated T_{FH} depletion. (A) Time-course of germinal center dissolution: *(i)* Serial sections of mesenteric LNs at Day 0, Day 1, and Day 6 following a single dose of Fc-silent anti-CD40L mAb (2 mg) stained for H&E, CD3, CD20, and PNA. Scale bars = 500 mm. *(ii–vi)* Quantitative morphometry in spleen and mesenteric LNs across Days 0, 1, and 6: total GC numbers *(ii)* (3 mice for

Days 0, 1 and 6 in spleen; 2 - 4 mice per time point in mesenteric LNs), individual GC cross-sectional areas *(iii)* (n = 12 GCs for Day 0, n = 12 GCs for Day 1, n = 2 GCs for Day 6 in spleen; n = 15 GCs for Day 0, n = 12 GCs for Day 1, and n = 0 GCs for Day 6 in mesenteric LNs), intra-GC $CD3^+$ T-cell density *(iv)*, T-cell zone area *(v)* (n = 9 - 12 fields per time point), and intra-TZ $CD3^+$ T-cell density *(vi)*. Welch's T-test; *p < 0.05, ** p < 0.01, ns = not significant. **(B) Combination regimen and *in vivo* tolerability:** *(i)* Treatment schedule: mice received anti-CD40L mAb on Day 0, followed by twice-daily CD3-IT on Days 1–4, IVS labeling, and tissue analysis on Day 6. *(ii)* Longitudinal body weight curves normalized to Day 0 (n = 5 for PBS; n = 3 for CD40L-mAb alone; n = 7 for 15 mg CD3-IT; n = 8 for combination). **(C) Depletion of follicular T cells following combination treatment:** Proportions of surviving $CD3^+$ T cells (% in CD45), $CD4^+$ T cells (% in CD45), and $CXCR5^+PD\text{-}1^{hi}$ T_{FH} cells (% in CD4) across spleen (IVS^-) and mesenteric LNs (IVS^-) in PBS (n = 6), CD40L-mAb alone (n = 4), 15 mg CD3-IT (n = 6), 25 mg CD3-IT (n = 4), and combination cohorts (n = 5-6). Treatment groups were compared with 25 µg CD3-IT using two-sided Welch's t-tests. Bars show mean ± SEM; adjusted p-values are displayed. **(D) Restoration of linear depletion kinetics:** Fold-reduction of T-cell subsets plotted against basal CD3epsilon MFI in mice treated with CD3-IT alone (top panels) versus anti-CD40L + CD3-IT combination (bottom panels) across peripheral blood, spleen, mesenteric LNs, and mandibular LNs (n = 6 PBS controls; n = 6 for 15 mg CD3-IT; n = 4 for 25 mg CD3-IT; n = 6 for combination). Dissolution of the GC realigns GC-T_{FH} (red filled dots) with the linear depletion trajectory.

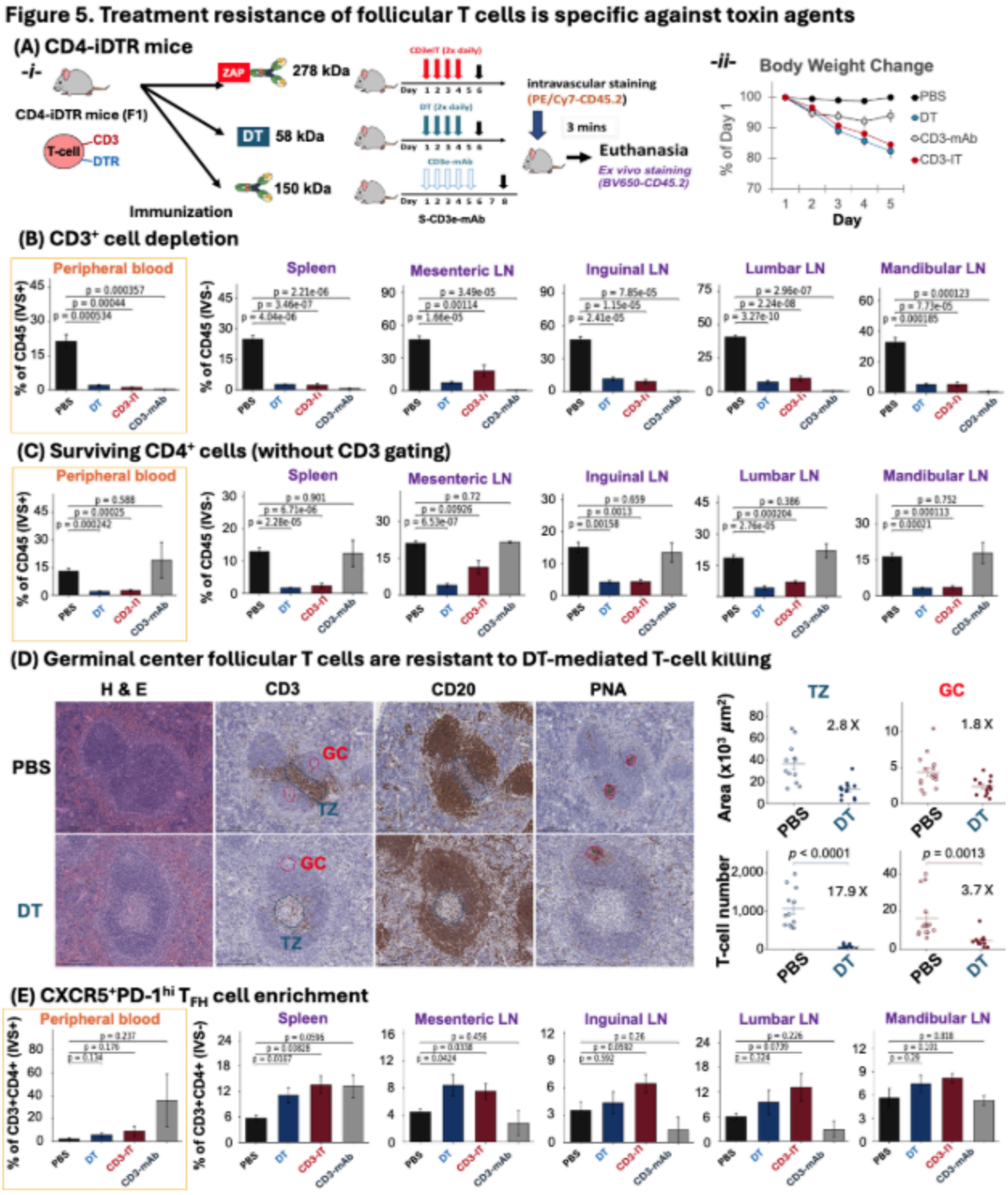


Figure 5

Cross-reagent profiling in CD4-iDTR mice reveals that germinal center protection is toxin-specific. (A) Transgenic comparative model and tolerability: *(i)* CD4-iDTR mice (expressing human diphtheria toxin receptors under the CD4 promoter) were treated with free DT (~58 kDa; 200 ng twice daily, Days 1–4), intact hamster anti-CD3 mAb (W-CD3-mAb; 40 mg daily, Days 1–5), Fc-silent anti-CD3 mAb (S-CD3-mAb; 40 mg daily, Days 1–5), or CD3-IT conjugate (~278 kDa; 25 mg twice daily, Days 1–4). *(ii)* Longitudinal body weight changes over 9 days (n = 10 for PBS; n = 11 for DT; n = 8 for CD3-IT; n = 7 for S-CD3-mAb).

(B-C) $CD3^+$ T cell depletion across lymphoid tissues(B)**:** Proportions of **$CD3^+$ T** cells among total **$CD45.2^+$** leukocytes in peripheral blood (IVS^+) and resident (IVS^-**)** fractions of the spleen and 5 lymph node chains (mesenteric, inguinal, mandibular, mediastinal, and lumbar). **Total $CD4^+$ T-cell frequencies**(C)**:** Frequencies of total **$CD4^+$ T** cells (analyzed without CD3 gating to account for antibody-induced CD3epsilon internalization) across indicated tissues. (n = 6-8 for PBS; n = 10-11 for DT; n = 6-7 for CD3-IT; n = 4 for S-CD3-mAb). **(D) Germinal center follicular T cells are relatively resistant to DT-mediated T-cell killing:** Immunohistochemistry of splenic follicles in PBS- and DT-treated CD4-iDTR mice stained for H&E, CD3, CD20, and PNA. Blue lines indicate TZs; red lines indicate GCs. Scatter plots show cross-sectional area (mm^2 x 10^3) and absolute T-cell numbers in TZs (n = 12 microscopic fields from 3 mice for PBS; n = 13 microscopic fields from 4 mice for DT) and GCs (n = 15 GCs from 3 mice for PBS; n = 13 GCs from 4 mice for DT). Two-sided unpaired Welch t-test; unadjusted; *$p < 0.05$, ** $p < 0.01$, ns = not significant. **(E) $CXCR5^+PD\text{-}1^{hi}$ T_{FH} cell enrichment:** Proportion of $CXCR5^+PD\text{-}1^{hi}$ cells among surviving tissue $CD4^+$ T cells across peripheral blood, spleen, mesenteric LNs, inguinal LNs, mandibular LNs, mediastinal LNs, and lumbar LNs (n = 4-6 for PBS; n = 4-9 for DT; n = 3-7 for CD3-IT; n = 3-4 for S-CD3-mAb). DT and CD3-IT induce significant **T_{FH}** enrichment, whereas S-CD3-mAb does not induce local LN enrichment.

Supplementary Files

This is a list of supplementary files associated with this preprint. Click to download.

- SupplementaryFigureLegends.docx